

Quark Number Susceptibility and QCD Phase Transition in the Predictive Soft-wall AdS/QCD Model with Finite Temperature

LING-XIAO CUI , SHINGO TAKEUCHI and YUE-LIANG WU

Kavli Institute for Theoretical physics China (KITPC)

Key Laboratory of Frontiers in Theoretical Physics

Institute of Theoretical Physics, Chinese Academy of Sciences, Beijing 100190, China

Abstract

Based on the infrared improved soft-wall AdS/QCD model which can lead to a consistent prediction for the mass spectra of light resonance mesons, we extend it to the finite temperature system and carry out the calculation for the quark number susceptibility with finite quark mass. As a consequence, we show that the quark number susceptibility grows rapidly with a continuous blow-up in a narrow temperature interval as the temperature increases, and there is a peak when the temperature is around $T \simeq 160 \sim 190$ MeV depending slightly on the models, the resulting critical temperature is about 170MeV, which agrees remarkably with the lattice QCD calculation.

1 Introduction

Quantum chromodynamics describes the dynamics of quarks. Its gauge group is non-Abelian and the gauged gluon fields have self-interactions. As a result, the beta-function at ultraviolet (UV) region becomes negative that leads to the asymptotic freedom [1,2]. While at low energies, the non-perturbative dynamics such as chiral symmetry breaking and linear confinement appear as the gauge coupling constant grows.

The duality between gravities and gauge theories [3-5] gives a new approach to the study of the low energy QCD. Among the studies of the duality, the ones developed phenomenologically are referred as bottom-up approach (AdS/QCD model) [6,7] (There are also good reviews, e.g. [8]). One of the important achievements in the AdS/QCD model are the realization of the chiral symmetry breaking in the hard-wall AdS/QCD model [6] and the linear confinement in the soft-wall AdS/QCD model [9]. But in the hard-wall model, the resulting excited meson mass spectra are found to be contrary to the experiments. In the soft-wall model, one can obtain desired mass spectra for the excited vector mesons, but the chiral symmetry breaking occurs inconsistently. Several groups studied on these problems [10,11]. A predictive soft-wall AdS/QCD model was constructed by simply modifying the 5D AdS metric in the infrared (IR) region [13] and the resulting mass spectra for the light resonance states of pseudoscalar, scalar, vector and axial-vector mesons remarkably agree with the experimental data. It is then interesting to study the phase transition for such a holographic AdS/QCD model with finite temperature, which comes to the purpose of our present paper. Thus we will extend such an infrared improved soft-wall AdS/QCD model [13] to a finite temperature system by considering a black hole metric and investigate the phase transition by computing the quark number susceptibility (QNS). The QNS is known to be the response of quark number density to infinitesimal change of the quark chemical potential as $\chi_q \equiv dn_q/d\mu_q$. Using the fluctuation-dissipation theorem, it can be expressed as [14]

$$\chi_q = - \lim_{k \rightarrow 0} \text{Re} G_{t\ t}^R(\omega = 0, k), \quad (1.1)$$

where $G_{t\ t}^R(\omega, k)$ is the two-point retarded Green function for time-component of quark number current. From the lattice QCD studies [15,16], it strongly suggests that the behavior of χ_q/T^2 on the transition between the hadronic phase and the Quark-Gluon-Plasma phase at zero quark chemical potential is a continuous but rapid in a narrow temperature interval around $T \simeq 170$ MeV [17]. In this paper, we are going to compute the QNS with the constituent quark mass \bar{m}_q due to the dynamically generated chiral condensation of quark $\sigma = \langle \bar{q}q \rangle$, which is defined as $\bar{m}_q = m_q + \sigma/\mu^2$ with m_q the current quark mass and σ/μ^2 regarded as the dynamically generated quark mass for the typical QCD scale $\mu \sim \Lambda_{QCD}$ due to QCD confinement [18], and to show how the behavior of χ_q/T^2 changes as the temperature and dynamical quark mass and what is the critical temperature at zero chemical potential.

This paper is organized as follows: in Sect.2, we present an introduction to our working model and the $U(1)$ gauge field dual to the quark number current. In Sect.3, we show how to get the quark number susceptibility from the solution of the $U(1)$ gauge field, and provide the numerical results with a detailed discussion. Our summary and remarks are presented in Sect.4.

2 The models

As the predictive soft-wall AdS/QCD model constructed by simply modifying the 5D AdS metric in the infrared (IR) region [13] can result the consistent mass spectra for the light resonance states of pseudoscalar, scalar, vector and axial-vector mesons, we shall extent such a model to a finite temperature system for studying the phase transition. This may simply be realized by considering a 5D black hole metric as follows

$$ds^2 = a^2(z) \left(f(z) dt^2 + \sum_{i=1}^3 dx_i^2 - \frac{dz^2}{f(z)} \right), \quad (2.1)$$

with

$$a^2(z) = 1/z^2 + \mu_g^2 \quad \text{and} \quad f(z) = 1 - (z/z_0)^4, \quad (2.2)$$

where z has the relation with the normal radial coordinate r as $z \equiv 1/r$ and z_0 is the horizon. The scale factor μ_g characterizes the confinement of QCD in the infrared region by breaking the conformal symmetry, it is fixed by fitting with a linear function for the excited states and has been given in [13] from a consistent prediction for the resonance meson mass spectra. Hawking temperature is given as $T = 1/(z_0\pi)$.

The action with the background dilaton $\Phi(z)$ which has a nontrivial solution for forming the soft-wall is given as [13]

$$S_{\Phi} = \int d^5x \sqrt{g} e^{-\Phi(z)} \text{Tr} \left(|D_M X(x, z)|^2 - m_X^2 |X(x, z)|^2 \right), \quad (2.3)$$

where $m_X^2 = -3$ so that the solution of dilaton $\Phi(z)$ obtained below does not have the singular at UV-limit ($z \rightarrow 0$). $X(x, z)$ is the bulk scalar field, and we denote its vacuum expectation value (VEV) as $X(z)$ for simplicity

$$X(z) = \frac{1}{2} v(z) \mathbf{1}_2, \quad (2.4)$$

where $\mathbf{1}_2$ denotes 2×2 unit matrix. For our purpose in the present note, we consider that the VEV $X(z)$ is taken as the same form given in [13], which is listed in Table.1. While, the dilaton $\Phi(z)$ is fixed from the equation of motion for $X(z)$ which is given as

$$0 = \partial_z \left(a^3(z) f(z) e^{-\Phi(z)} \partial_z v(z) \right) - a^5(z) e^{-\Phi(z)} m_X^2 v(z). \quad (2.5)$$

where the resulting $\Phi(z)$ from eq.(2.5) will be different from the one yielded in [13] due to the inclusion of the black hole metric $f(z)$.

Model	$v(z)$	Parameters
Ia	$z(A + Bz^2)(1 + Cz^2)^{-1}$	$B = \sigma/\zeta + m_q\zeta C, \quad C = B/(\mu_d\gamma)$
Ib	$z(A + Bz^2)(1 + Cz^2)^{-5/4}$	$B = \sigma/\zeta + \frac{5}{4}m_q\zeta C, \quad C = (B^2/(\mu_d\gamma^2))^{2/5}$
IIa	$z(A + Bz^2)(1 + Cz^4)^{-1/2}$	$B = \sigma/\zeta, \quad C = (B/(\mu_d\gamma))^2$
IIb	$z(A + Bz^2)(1 + Cz^4)^{-5/8}$	$B = \sigma/\zeta, \quad C = (B^2/(\mu_d\gamma^2))^{4/5}$

Table 1: $A = m_q\zeta$ and $\zeta = \sqrt{3}/(2\pi)$ for all the models, while $\mu_d^2 \equiv 3/(2\alpha)\mu_g^2$ with $\alpha = 1$ for the Ia, IIa and $\alpha = 1/2$ for the Ib, IIb. A, B and C satisfy eq.(2.7). Numerical values of m_q, γ and σ are given in Table.2.

Such an VEV may be regarded as the one at the low temperature phase. It was shown that the boundary behaviors of the VEV play an essential role [13] for mass spectra of resonances mesons. In general, its UV boundary behavior is fixed by the AdS/CFT correspondence, while its IR boundary behavior is imposed so as to obtain the required boundary behavior of dilaton at the IR-region. From Table.1, we can see that $v(z)$ behaves in the IR-limit $z \rightarrow \infty$ and the UV-limit $z \rightarrow 0$ as

$$v(z)|_{z \rightarrow \infty} = \gamma \left(\sqrt{\frac{3}{2\alpha}} \mu_g z \right)^\alpha \equiv \gamma (\mu_d z)^\alpha, \quad (2.6)$$

$$v(z)|_{\text{UV-limit}} = m_q \zeta z + \frac{\sigma}{\zeta} z^3. \quad (2.7)$$

where μ_d^2 is defined with $\alpha = 1$ for the Model Ia and IIa and $\alpha = 1/2$ for the Model Ib and IIb, and ζ is fixed as $\zeta = \sqrt{3}/(2\pi)$ [13]. m_q and σ denote the current quark mass and the chiral condensation respectively, and the constituent quark mass in this paper is defined as $\bar{m}_q = m_q + \sigma/\mu^2$ [18]. Their numerical values are given in Table.2, which have been fixed by minimizing the breaking of the Gell-Mann-Oakes-Renner relation as

$$f_\pi^2 m_\pi^2 = 2m_q \sigma \quad (2.8)$$

at the 1% level and the experimental values: $m_\pi = 139.6$ MeV and $f_\pi = 92.4$ MeV.

To compute QNS by using eq.(1.1), let us now introduce an $U(1)$ gauge field which is dual to the 4D quark number current. Changing the coordinate to $u \equiv (z/z_H)^2$, and considering the following action

$$S = -\frac{1}{4g_5^2} \int dud^4x \sqrt{g} e^{-\Phi(u)} F_{mn} F^{mn}. \quad (2.9)$$

we can simply get the equation of motion $0 = \partial_\mu(\sqrt{g}e^{-\Phi}F^{\mu\nu})$ for A_ν . Performing the Fourier transformation as $A_\mu(t, x, u) = \int \frac{d^4k}{(2\pi)^4} e^{-i\omega t + i\mathbf{x}k} \tilde{A}_\mu(\omega, k, u)$, choosing the momenta k along the x -direction and

Model	Ia	Ib	IIa	IIb
m_q (MeV)	4.16	4.64	4.44	4.07
$\sigma^{\frac{1}{3}}$ (MeV)	275	265	265	272
γ	0.178	0.136	0.153	0.112

Table 2: $\mu_d^2 \equiv 3/(2\alpha)\mu_g^2 = 445^2$ with $\alpha = 1$ for the Ia, IIa and $\alpha = 1/2$ for the Ib, IIb.

taking the axial gauge $A_u(u) = 0$, we obtain the following equations of motion for the needed components

$$A_t : 0 = (e^{-\Phi} \sqrt{g} g^{uu} g^{tt} A_t')' - q^2 e^{-\Phi} \sqrt{g} g^{xx} g^{tt} A_t - \omega q e^{-\Phi} \sqrt{g} g^{xx} g^{tt} A_z, \quad (2.10)$$

$$A_u : 0 = \omega g^{tt} A_t' - q g^{xx} A_z', \quad (2.11)$$

where q and ω are defined as $q \equiv k/(2\pi T)$ and $\omega \equiv w/(2\pi T)$, the prime denotes derivative with regard to u , and in this study we use x -direction as a usual z -direction in four dimensional space-time due to what we have already used the symbol z as the fifth dimension here. In the above equations, we represent \tilde{A}_μ as A_μ , and will apply this manner in this paper for simplicity.

3 The results

It turns out that the solution $\Phi(u)$ can be obtained analytically from the equation of motion eq.(2.5) for all the models*. In obtaining the solution for the dilaton $\Phi(u)$, we take the integral constant so that the solution at the boundary behaves as

$$\Phi(z)|_{\text{UV-limit}} = 3\mu_g^2 z^2, \quad (3.1)$$

Here we abbreviate to represent its explicit results due to a long expression. By using the solutions $\Phi(u)$ in all the models and the equation of motion eq.(2.10), we are able to get the retarded green function.

From eq.(2.10), we can obtain the following equation

$$0 = \left(\frac{\psi'}{e^{-\Phi} \sqrt{g} g^{xx} g^{tt}} \right)' - \left(\frac{\omega^2 g^{tt} / g^{xx} + q^2}{e^{-\Phi} \sqrt{g} g^{uu} g^{tt}} \right) \psi \quad (3.2)$$

with $\psi \equiv e^{-\Phi} \sqrt{g} g^{uu} g^{tt} A_t'$. Note that there is a singular at $u = 1$ due to the horizon, and the deepest one is with the power -2 . To get rid of such a singular, we assume that the solution of ψ has the form $\psi = (1 - u)^{i\nu\omega} X(u, \omega, q)$ with the regular function $X(u, \omega, q)$. Then by appropriately determining the index ν , we can regularize the singular behavior. In general, there are two options for the values of ν , which corresponds to the in-going and out-going solutions respectively. In our present consideration, as

*We use mathematica 8.

the value of ω is taken to be zero eventually following eq.(1.1), it is not important to specify which one we are actually taking. In the following treatments, we consider the case that $\omega, q \ll 1$ in the hydrodynamic expansion. With such an assumption, the form of the function $X(u, \omega, q)$ can be expressed in the general form: $X(u, \omega, q) = \psi_0 + q^2\psi_1(u) + \omega^2\psi_2(u) + \mathcal{O}(\omega^4, q^4)$. As a result, provided that $\nu \rightarrow 0$ for $\omega \rightarrow 0$, we can show that ψ_0 and ψ_1 satisfy the following equations

$$0 = \left(\frac{\psi'_0}{e^{-\Phi} \sqrt{g} g^{xx} g^{tt}} \right)', \quad (3.3)$$

$$0 = \left(\frac{\psi'_1}{e^{-\Phi} \sqrt{g} g^{xx} g^{tt}} \right)' - \frac{\psi_0}{e^{-\Phi} \sqrt{g} g^{uu} g^{tt}}. \quad (3.4)$$

It is then not difficult to find out the solution for ψ_0

$$\psi_0 = C_1 + C_2 \int_1^u du e^{-\Phi} \sqrt{g} g^{xx} g^{tt}. \quad (3.5)$$

as the integrand $\sqrt{g} g^{xx} g^{tt}$ has the singularity arising from the horizon, we then take $C_2 = 0$. And the solution for ψ_1 is given

$$\psi'_1 = C_1 e^{-\Phi} \sqrt{g} g^{xx} g^{tt} \left(\int_1^u du' \frac{1}{e^{-\Phi} \sqrt{g} g^{uu} g^{tt}} + D_1 \right), \quad (3.6)$$

From the condition $\psi'(u=1) = 0$, the integral constant D_1 can be fixed. From the A_t -component of eq.(2.10) and the definition of ψ with $\omega \rightarrow 0$, we have

$$A_t = C_1 \left(\int_1^u du' \frac{1}{e^{-\Phi} \sqrt{g} g^{uu} g^{tt}} + D_1 \right) + \mathcal{O}(\omega^2, q^2). \quad (3.7)$$

where C_1 can be fixed by using $\lim_{u \rightarrow 0} A_t \equiv A_t^{(0)}$ to be

$$C_1 = A_t^{(0)} \left(\int_1^0 du' \frac{1}{e^{-\Phi} \sqrt{g} g^{uu} g^{tt}} + D_1 \right)^{-1} + \mathcal{O}(\omega^2, q^2). \quad (3.8)$$

Here, $A_t^{(0)}$ plays the role as the source for the 4D quark number current mentioned in the above eq.(2.9).

From the definition of ψ , we can obtain the following expression

$$A'_t = \frac{C_1}{e^{-\Phi} \sqrt{g} g^{uu} g^{tt}} + \mathcal{O}(\omega^2, q^2) + \mathcal{O}(\omega^2, q^2). \quad (3.9)$$

We now come to discuss the retarded green function through the GKP-W relation [4, 5] and the prescription [12]. It turns out that the on-shell action takes

$$S_0 = \frac{e^{-\Phi} \sqrt{g} g^{uu} g^{tt}}{2g_5^2} \int \frac{d^4 k}{(2\pi)^4} \left(A_t A'_t - \frac{1}{f} A_x A'_x \right) \Big|_{u=1}^0. \quad (3.10)$$

Thus the retarded green function G_t^R is found to be

$$G_t^R(m_q, \mu_d, \sigma) = -\frac{1}{g_5^2} \left(\int_1^0 du \frac{1}{e^{-\Phi} \sqrt{g} g^{uu} g^{tt}} + D_1 \right)^{-1} + \mathcal{O}(\omega^2, q^2), \quad (3.11)$$

where $A_t^{(0)}$ is normalized to 1. By taking $q \rightarrow 0$ with $\omega = 0$, we can obtain the quark number susceptibility χ_q through eq.(1.1). In the following computation, we will neglect the high order correction part of $\mathcal{O}(\omega^2, q^2)$, and also take g_5 to be $g_5 = 1$ for simplicity as the physics property of the green function $G_{t t}^R$ is irrelevant to its absolute value.

We shall compute χ_q/T^2 as function of three parameters σ , m_q and μ_d . Typically, we will discuss the variation of σ with a range ± 25 toward the value of $\sigma^{1/3}$ in Table.2. This does not mean the uncertainty but the range to see how the QNS χ_q/T^2 changes as the dynamical quark mass. On the other hand, we shall consider the uncertainty of about 10% toward the values of μ_d in Table.2, which is mainly caused from the difference between the predicted mass spectra and experimental data for the resonance meson states [13].

Ia :	$\sigma^{1/3} = 275 \pm 25$ ($m_q \simeq 4.16 \mp 1.2$), $\gamma = 0.178$ and $\mu_d = 445$ ($\mu_g = 363$)
Ib :	$\sigma^{1/3} = 265 \pm 25$ ($m_q \simeq 4.64 \mp 1.2$), $\gamma = 0.178$ and $\mu_d = 445$ ($\mu_g = 257$)
IIa :	$\sigma^{1/3} = 265 \pm 25$ ($m_q \simeq 4.44 \mp 1.2$), $\gamma = 0.178$ and $\mu_d = 445$ ($\mu_g = 363$)
IIb :	$\sigma^{1/3} = 272 \pm 25$ ($m_q \simeq 4.07 \mp 1.2$), $\gamma = 0.178$ and $\mu_d = 445$ ($\mu_g = 257$)

Table 3: The parameters used in Fig.2. γ is dimensionless and the unit of the rest are MeV. m_q is automatically fixed by the relation.(2.8).

Ia :	$m_q = 4.16$, $\sigma^{1/3} = 275$, $\gamma = 0.178$ and $\mu_d = 445 \pm 50$ ($\mu_g \simeq 363 \mp 40$)
Ib :	$m_q = 4.64$, $\sigma^{1/3} = 265$, $\gamma = 0.136$ and $\mu_d = 445 \pm 50$ ($\mu_g \simeq 257 \mp 30$)
IIa :	$m_q = 4.44$, $\sigma^{1/3} = 265$, $\gamma = 0.153$ and $\mu_d = 445 \pm 50$ ($\mu_g \simeq 363 \mp 40$)
IIb :	$m_q = 4.07$, $\sigma^{1/3} = 272$, $\gamma = 0.112$ and $\mu_d = 445 \pm 50$ ($\mu_g \simeq 257 \mp 30$)

Table 4: The parameters used in Fig.3. γ is dimensionless and the unit of the rest are MeV. The relation for μ_d^2 and μ_g^2 are given in eq.(2.6).

Before making the computation of quark number susceptibility, we may check that the solutions A_t' are well-defined in the entire bulk (Fig.1).

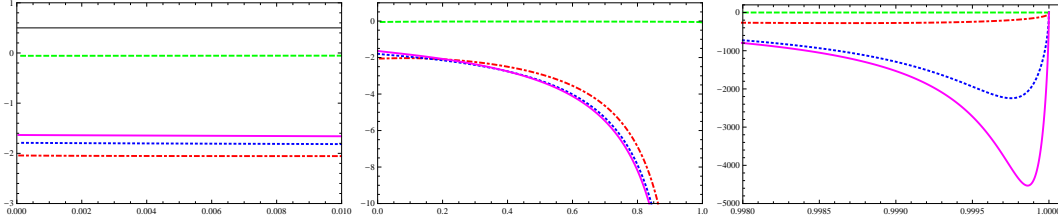


Figure 1: The figures show the regularity of the solution A'_t in the entire bulk. Note the scale taken in each figures. The x-axis and y-axis denote the radial coordinate u and the real part of the solution A'_t in the Ia model, respectively. On the other hand, the imaginary-part in all models always takes the value extremely close to zero. Considering it as just a numerical error, we then skip to show it here. The three figures are for the real-part of the model Ia: the left one indicates no-UV divergence, the center one shows the behavior in the whole region, and the right one shows finiteness and the boundary condition is taken correctly around the horizon. The behaviors for other models are the same. In the figures, we have taken $u \in [10^{-25}, 1 - 10^{-10}]$ with the in-going boundary condition, and q and ω are taken to be zero. The parameters used here are given in Table.4 with temperature changing as $T=120$ (green, dashed), $T=200$ (red, dot-dashed), $T=300$ (blue, dotted), $T=400$ (magenta, solid), (Unit is MeV).

From the results shown in Fig.1, it is seen that there is no divergence involved in our present considerations, therefore we do not need to care the regularization for the retarded green function [19, 20]. Thus by using the parameters in Table.3 and 4, we obtain the results shown in Fig.2 and 3.

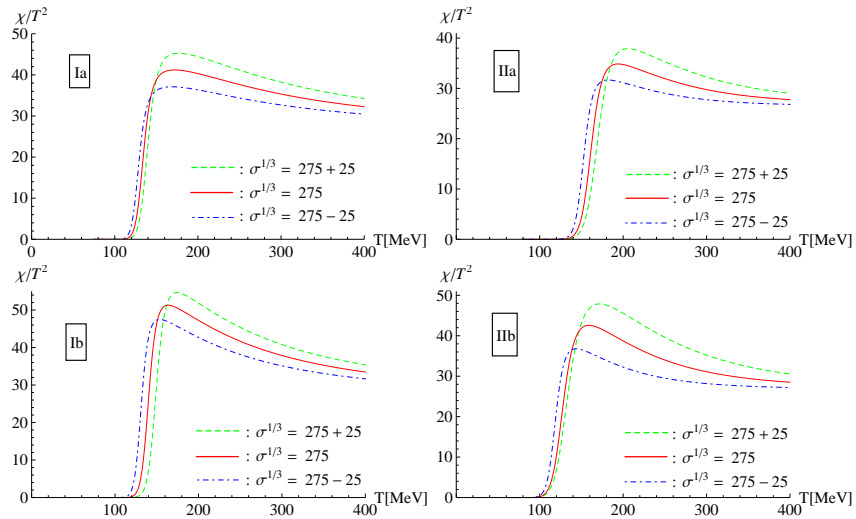


Figure 2: Results with fixing μ_d and varying m_q and $\sigma^{1/3}$ as in Table.3. The different curves from top to bottom in all figures correspond to $\sigma^{1/3} = 275 + 25$ (green, dashed), $\sigma^{1/3} = 275$ (red, solid) and $\sigma^{1/3} = 275 - 25$ (blue, dot-dashed). The changes of σ is just to see the dependence of QNS on the constituent quark mass given by $\bar{m}_q = m_q + \sigma/\mu^2$. It is observed that the appearing of peaks and its locations in all models agree with the results of lattice QCD [16].

It can be seen from Figs.2 and 3 that the QNS χ_q/T^2 emerges rapidly with a continuous blow-up in a narrow temperature interval as the temperature increases. There is a peak when the temperature reaches to be around $T \sim 160 \sim 190$ MeV depending slightly on models, and after that, the behaviors of χ_q/T^2 get slowly in all the models. As mentioned in the introduction, the results of lattice QCD [15, 16]

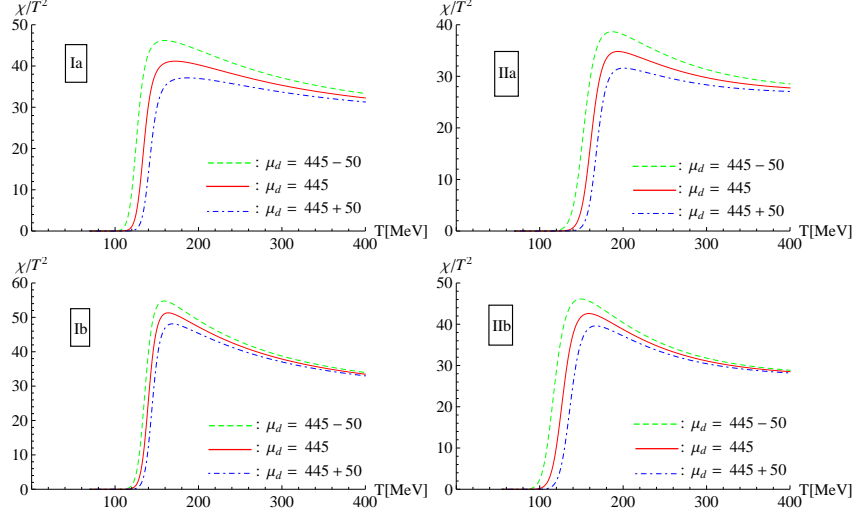


Figure 3: Results with fixing m_q and $\sigma^{1/3}$ as in Table.4 and varying μ_d . The different curves from top to bottom in all figures correspond to $\mu_d = 445 - 50$ (green, dashed), $\mu_d = 445$ (red, solid) and $\mu_d = 445 + 50$ (blue, dot-dashed). The possible differences with regard to μ_d arise from the one between the predicted resonance meson mass spectra and the experimental data. It can be seen that the appearing of peaks and its locations in all models are in good agreement with the lattice QCD' results. [16].

have shown that when the phase changes from the hadron phase to the quark-gluon-plasma phase at zero chemical potential, χ_q/T^2 grows rapidly and continuously with a peak around $T \simeq 170$ MeV. Therefore, the appearing of peaks and its locations in all models are in good agreement with the lattice QCD' results

Let us now make a determination for the critical temperature in each model, which is simply fixed at the location of the peak

$$\text{Ia} : T_c = 173.6 \pm 3.2 \Big|_{\sigma^{1/3}} \pm 11.7 \Big|_{\mu_d}, \quad (3.12)$$

$$\text{Ib} : T_c = 164.4 \pm 8.1 \Big|_{\sigma^{1/3}} \pm 5.2 \Big|_{\mu_d}, \quad (3.13)$$

$$\text{IIa} : T_c = 194.9 \pm 7.4 \Big|_{\sigma^{1/3}} \pm 9.2 \Big|_{\mu_d}, \quad (3.14)$$

$$\text{IIb} : T_c = 159.5 \pm 7.8 \Big|_{\sigma^{1/3}} \pm 9.4 \Big|_{\mu_d}, \quad (3.15)$$

where the uncertainties come from the quantities $|\sigma^{1/3}$ and $|\mu_d$ as denoted by the subindices, the possible variations of $|\sigma^{1/3}$ and $|\mu_d$ are given in Tables3 and 4.

From the above analysis and results, we would like to address the following points: First, we may draw attention to the effect of the VEV $v(z)$. From Fig.2, it is seen that the effects in all models are similar as long as it satisfies the boundary conditions (2.6) and (2.7) with the given α , regardless of the form of $v(z)$. On the other hand, it turns out that the appearing of the peaks moves to high temperature as $\sigma^{1/3}$ increases. Next, let us turn to the effects of μ_g^2 . From Fig.3, it is noticed that the behaviors of the peak become softer in all models, and the locations of the peak shift to the high temperature as μ_g^2 increases.

As for the effect of quark mass, considering the constituent quark mass defined via $\bar{m}_q = m_q + \sigma/\mu^2$ with m_q and σ/μ^2 denoting the current quark mass and the dynamically generated quark mass via chiral condensation, respectively. As the relation eq.(2.8) is kept to be held, the current quark mass m_q and the dynamically generated quark mass or chiral condensation σ are varying oppositely, which can be seen explicitly from Table.3. It can also be seen from Fig.2 that when the constituent quark mass \bar{m}_q is going to be increased, which is toward the increased σ associated with the decreased m_q due to the relation eq.(2.8), the behavior of the QNS is getting steeper, and vice versa. This is consistent with the general point of view that the more massive the current quark mass becomes, the more moderate the behavior of the peak for the QNS χ/T^2 gets. In this sense, it can be interpreted that the effect of current quark mass m_q is more effective than the one of dynamically generated quark mass or the chiral condensation σ . Finally, we plot in Fig.4 the results in all models with parameters given in Table.2 and the temperature is normalized by the critical temperature T_c , so that each peak denoting T_c come to 1 on the x-axis.

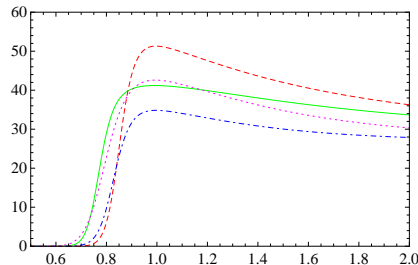


Figure 4: The results of all models with the parameters given in Table.2. The curves corresponding to different models may be distinguished from their locations corresponding to large value of $T/T_c \geq 1.5$, from top to bottom, they are: Ib (red, dashed), Ia (green, solid), IIb (Magenta, dashed), IIa (blue, dot-dashed). The x-axis and y-axis denote the normalized temperature T/T_c and χ/T^2 , respectively.

4 Summary and Remarks

In this paper, we have extended the predictive soft-wall AdS/QCD model [13] to a finite temperature system and carried out the calculation for the quark number susceptibility with finite quark mass. It has been shown that the critical behaviors in all models agree well with the lattice QCD calculation [15,16]. This further demonstrates that the predictive soft-wall AdS/QCD model proposed in [13] is a reasonable and realistic effective model for describing the QCD confinement and chiral symmetry breaking, where the conformal symmetry breaking at infrared region due to nonperturbative QCD effects is characterized by the modified infrared behavior of metric parameterized by μ_g^2 in the metric and the nontrivial dilaton background (namely the soft-wall) which is determined by both the IR parameter μ_g^2 and the VEV $v(z)$. It seems reasonable to suppose that $v(z)$ has almost the same effects as long as it satisfies the boundary

condition (2.6) and (2.7). In addition, it has been noticed that the critical temperature is put to a low temperature by the soft-wall, while the effect of IR behavior μ_g^2 will pull it up to high temperature. Thus the matching of the critical behaviors can be seen as the result of a very fine balance between μ_g^2 and the soft-wall. As for the effect of quark mass given by the constituent quark mass $\bar{m}_q = m_q + \sigma/\mu^2$, it has been shown that the effect of current quark mass m_q is more significant than the one of chiral condensation σ or dynamically generated quark mass when the relation eq. (2.8) is imposed, which may be explicitly seen from the relation $\bar{m}_q = m_q + f_\pi^2 m_\pi^2 / (2m_q \mu^2)$.

Here we only consider two flavors, it would be interesting to investigate the nature of QCD transition with three flavor case, and also with including the chemical potential. On the other hand, the quartic interaction term of the scalar field has been dropped in eq.(2.3), while it has been shown that it has a sizable role in the computation of the mass spectra of resonance mesons [13]. Also the back reaction effects of the dilaton field and gravity may be the core in the improvement of our model [21]. We shall consider those interesting topics in our future studies.

Acknowledgments

The authors would like to thank Y.B. Yang for useful discussions. This work is supported in part the National Nature Science Foundation of China (NSFC) under Grants No. 10975170, No. 10821504 and No. 10905084; and the Project of Knowledge Innovation Program (PKIP) of the Chinese Academy of Science.

References

- [1] D. J. Gross and F. Wilczek, Phys. Rev. Lett. **30**, 1343 (1973).
- [2] H. D. Politzer, Phys. Rev. Lett. **30**, 1346 (1973).
- [3] J. M. Maldacena, Adv. Theor. Math. Phys. **2**, 231 (1998) [Int. J. Theor. Phys. **38**, 1113 (1999)] [arXiv:hep-th/9711200].
- [4] S. S. Gubser, I. R. Klebanov and A. M. Polyakov, Phys. Lett. B **428**, 105 (1998) [arXiv:hep-th/9802109].
- [5] E. Witten, Adv. Theor. Math. Phys. **2**, 253 (1998) [arXiv:hep-th/9802150].
- [6] J. Erlich, E. Katz, D. T. Son and M. A. Stephanov, Phys. Rev. Lett. **95**, 261602 (2005) [arXiv:hep-ph/0501128].
- [7] L. Da Rold and A. Pomarol, Nucl. Phys. B **721** (2005) 79 [arXiv:hep-ph/0501218].

- [8] Y. Kim, D. Yi, [arXiv:1107.0155 [hep-ph]].; T. M. Kelley, [arXiv:1108.0653 [hep-ph]].
- [9] A. Karch, E. Katz, D. T. Son and M. A. Stephanov, Phys. Rev. D **74**, 015005 (2006) [arXiv:hep-ph/0602229].
- [10] T. Gherghetta, J. I. Kapusta and T. M. Kelley, Phys. Rev. D **79** (2009) 076003 [arXiv:0902.1998 [hep-ph]].
- [11] P. Colangelo, F. De Fazio, F. Giannuzzi, F. Jugeau and S. Nicotri, Phys. Rev. D **78** (2008) 055009 [arXiv:0807.1054 [hep-ph]].
- [12] G. Policastro, D. T. Son and A. O. Starinets, JHEP **0209**, 043 (2002) [arXiv:hep-th/0205052].
- [13] Y. Q. Sui, Y. L. Wu, Z. F. Xie and Y. B. Yang, Phys. Rev. D **81**, 014024 (2010) [arXiv:0909.3887 [hep-ph]].
Y. Q. Sui, Y. L. Wu and Y. B. Yang, Phys. Rev. D **83**, 065030 (2011).
- [14] T. Kunihiro, Phys. Lett. **B271** (1991) 395.
- [15] L. McLerran, Phys. Rev. **D36** (1987) 3291.
- [16] C. R. Allton *et al.*, Phys. Rev. D **66**, 074507 (2002) [arXiv:hep-lat/0204010].
C. R. Allton, S. Ejiri, S. J. Hands, O. Kaczmarek, F. Karsch, E. Laermann and C. Schmidt, Phys. Rev. D **68**, 014507 (2003) [arXiv:hep-lat/0305007].
C. R. Allton *et al.*, Phys. Rev. D **71**, 054508 (2005) [arXiv:hep-lat/0501030].
- [17] see for instance: F. Karsch, Lect. Notes Phys. **583** (2002) 209.
- [18] Y. B. Dai and Y. L. Wu, Eur. Phys. J. C **39** (2004) S1 [arXiv:hep-ph/0304075].
- [19] K. I. Kim, Y. Kim, S. Takeuchi and T. Tsukioka, to appear in Prog. Theor. Phys. **126** (2011) arXiv:1012.2667 [hep-ph].
Y. Kim, Y. Matsuo, W. Sim, S. Takeuchi and T. Tsukioka, JHEP **1005**, 038 (2010) [arXiv:1001.5343 [hep-th]].
- [20] Y. Matsuo, S. J. Sin, S. Takeuchi and T. Tsukioka, JHEP **1004** (2010) 071 [arXiv:0910.3722 [hep-th]].
Y. Matsuo, S. J. Sin, S. Takeuchi, T. Tsukioka and C. M. Yoo, Nucl. Phys. B **820**, 593 (2009) [arXiv:0901.0610 [hep-th]].
- [21] J. P. Shock, F. Wu, Y. L. Wu and Z. F. Xie, JHEP **0703** (2007) 064 [arXiv:hep-ph/0611227].
Y. L. Wu and Z. F. Xie, JHEP **0710** (2007) 009 [arXiv:0705.2360 [hep-ph]].